Journal of Biomechanics 58 (2017) 52–63

Contents lists available at ScienceDirect

Journal of Biomechanics

journal homepage: www.elsevier.com/locate/jbiomech
www.JBiomech.com

Twente spine model: A complete and coherent dataset for musculo-skeletal modeling of the thoracic and cervical regions of the human spine

Riza Bayoglu [a,*], Leo Geeraedts [b], Karlijn H.J. Groenen [c], Nico Verdonschot [a,c], Bart Koopman [a], Jasper Homminga [a]

[a] Department of Biomechanical Engineering, University of Twente, P.O. Box 217, 7500 AE Enschede, The Netherlands
[b] Radboud University Medical Center, Department of Anatomy, Nijmegen, The Netherlands
[c] Radboud University Medical Center, Radboud Institute for Health Sciences, Orthopaedic Research Laboratory, Nijmegen, The Netherlands

ARTICLE INFO

Article history:
Accepted 9 April 2017

Keywords:
Thoracic spine
Cervical spine
Cadaver
Musculo-skeletal model
Muscles
PCSA
Sarcomere length
Optimal-fiber length

ABSTRACT

Musculo-skeletal modeling could play a key role in advancing our understanding of the healthy and pathological spine, but the credibility of such models are strictly dependent on the accuracy of the anatomical data incorporated. In this study, we present a complete and coherent musculo-skeletal dataset for the thoracic and cervical regions of the human spine, obtained through detailed dissection of an embalmed male cadaver. We divided the muscles into a number of muscle-tendon elements, digitized their attachments at the bones, and measured morphological muscle parameters. In total, 225 muscle elements were measured over 39 muscles. For every muscle element, we provide the coordinates of its attachments, fiber length, tendon length, sarcomere length, optimal fiber length, pennation angle, mass, and physiological cross-sectional area together with the skeletal geometry of the cadaver. Results were consistent with similar anatomical studies. Furthermore, we report new data for several muscles such as rotatores, multifidus, levatores costarum, spinalis, semispinalis, subcostales, transversus thoracis, and intercostales muscles. This dataset complements our previous study where we presented a consistent dataset for the *lumbar* region of the spine (Bayoglu et al., 2017). Therefore, when used together, these datasets enable a complete and coherent dataset for the entire spine. The complete dataset will be used to develop a musculo-skeletal model for the entire human spine to study clinical and ergonomic applications.

1. Introduction

Musculo-skeletal models provide clinically useful information for understanding the normal and pathological functioning of the spine (Erdemir et al., 2007; Arjmand et al., 2009). Once validated, such models are valuable tools which can optimize surgical interventions and improve current treatment techniques (de Zee et al., 2007; Bruno et al., 2015; Arshad et al., 2016; Ignasiak et al., 2016). For example, the effect of posture on spinal loads and muscle forces can be explored (Briggs et al., 2007) or the effect of resection of muscles on the activity of other muscles can be studied before a spinal surgery so that an effective approach is planned (Bresnahan et al., 2010).

Previous anatomical studies on the spine mainly focused on the cervical and lumbar regions. Kamibayashi and Richmond (1998) measured the morphological parameters of some neck muscles from several cadavers, and Borst et al. (2011) measured muscle attachment sites and the morphological parameters of *all* neck muscles from a single cadaver. Other studies dissected muscles from the lumbar spine, presented anatomical drawings to illustrate muscle attachments, and measured the morphological parameters (Bogduk et al., 1992a,b, 1998; Macintosh and Bogduk, 1991; Macintosh et al., 1986; Delp et al., 2001; Phillips et al., 2008). To the knowledge of the authors, there is, however, no anatomical dataset which enables developing a complete and coherent musculo-skeletal model for the entire human spine. The lack of such coherent musculo-skeletal data requires current models to combine data from several cadavers. This approach then necessitates anatomical scaling between the skeletal geometries of the spines and the muscle architectures of the cadavers. As a result, models may contain musculo-skeletal systems that are not anatomically realistic. A musculo-skeletal dataset measured from a single body will enable a complete and consistent model of the

* Corresponding author. Fax: +31 53 489 2287.
E-mail address: r.bayoglu@hotmail.com (R. Bayoglu).

http://dx.doi.org/10.1016/j.jbiomech.2017.04.003
0021-9290/

spine and is, therefore, a better approach for clinical practice (Carbone et al., 2015).

Accuracy on modeling lines-of-action and architectural parameters of muscles in musculo-skeletal models is of critical importance to yield reliable muscle and joint force estimations. Previous studies showed that models are very sensitive to the geometry of the spine (Han et al., 2013; Putzer et al., 2016) and the changes in muscle attachment sites (Carbone et al., 2012). Furthermore, morphological (architectural) parameters such as fiber length, sarcomere length, optimal fiber length, tendon length, pennation angle, mass, and physiological cross-sectional area affect model predictions significantly (Arnold et al., 2010; Valente et al., 2014; Carbone et al., 2016; Modenese et al., 2016). These morphological parameters will facilitate more realistic simulation of muscle contraction dynamics in such models and, thus, will increase their credibility (Zajac, 1989; Vasavada et al., 1998).

In our previous study, we presented a complete and coherent musculo-skeletal dataset for modeling the *lumbar* region of the spine (Bayoglu et al., 2017). Thus, the aim of this study is to obtain a complete and coherent musculo-skeletal dataset for modeling the thoracic and cervical regions of the spine. We provide segmented bone surfaces, three-dimensional coordinates of muscle attachment sites, and the morphological muscle parameters measured from the same cadaver as in our previous study. When these two datasets are combined, a complete and consistent musculo-skeletal model of the entire spine can be developed. The complete dataset is freely available through https://www.utwente.nl/en/et/bw/research/projects/twentespinemodel.

2. Materials and methods

We obtained an embalmed human cadaver body (79 years-old male, height: 154 cm, mass: 51 kg) with institutional approval from Radboud university medical center. The cause of death was Alzheimer. We noticed slight scoliosis around the cadaver's neck (see Fig. 1d). In the cadaver, we distinguished 43 bones: seven cervical, twelve thoracic, and four lumbar vertebrae, twelve ribs, skull, sternum, clavicle, scapula, hyoid, thyrohyoid, sacrum, and pelvis.

We measured muscles of the thoracic and cervical regions of the spine from the right side of the cadaver. The experimental method consisted of two parts and was described in detail in our previous study (Bayoglu et al., 2017). In the first part, we divided the muscles into a number of muscle-tendon elements to represent their function effectively. Subsequently, we dissected the muscle elements and measured the positions of their attachments at origin and insertion by using the NDI Hybrid Polaris Spectra tracking system. We additionally measured the positions of via points for elements with a curved lines-of-action. Muscle attachments were measured with respect to the corresponding reference frames of the bones, registered with the segmented CT images, and finally expressed with respect to the global reference frame (see Fig. 1a and b). The global reference frame was defined by the CT scanner, and in this frame *x*-, *y*-, and *z*-axes point laterally (to the left side of the cadaver), posteriorly, and cranially, respectively (see Fig. 1d). This reference frame (Cartesian coordinate system) used for reporting the coordinates is the same as the one used in our earlier study (Bayoglu et al., 2017). Finally, we labeled the resected elements and stored them in 2% formaldehyde solution until the measurement of the morphological parameters. In the second part, we measured the following morphological muscle parameters for every element: fiber length, tendon length, optimal fiber length, pennation angle, mass, and physiological cross-sectional area. An average sarcomere length was measured for every muscle by using the laser diffraction method (Cross et al., 1981) (see Fig. 1c).

The resection protocol was slightly different for longissimus cervicis, semispinalis thoracis, iliocostalis thoracis, and longissimus capitis muscles. For these muscles, firstly, attachments at the bones were measured, and the entire muscle was resected afterward. Subsequently, muscles were micro-dissected and were divided into elements.

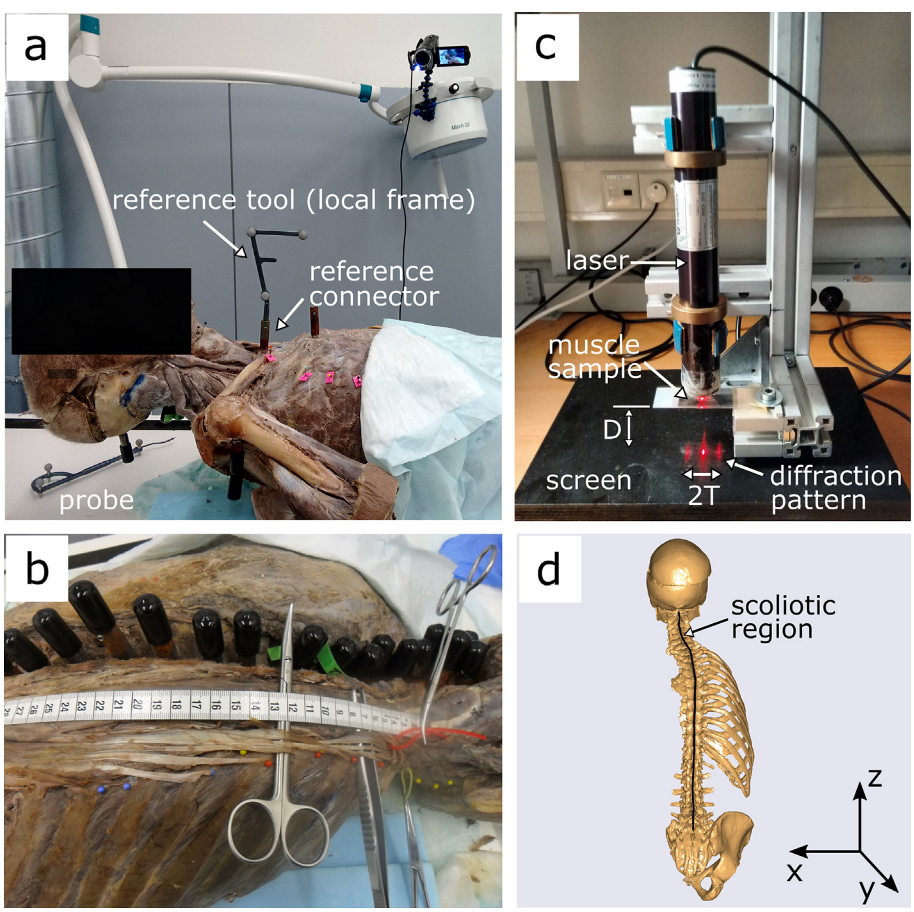

Fig. 1. (a) An instance during position measurements showing the reference frames used for the bones and the probe. (b) Locating attachments of erector spinae muscle group. (c) Laser diffraction set-up used for sarcomere length measurements. (d) Visualization of scoliosis in the cadaver. A curve which connects the spinous processes was drawn.

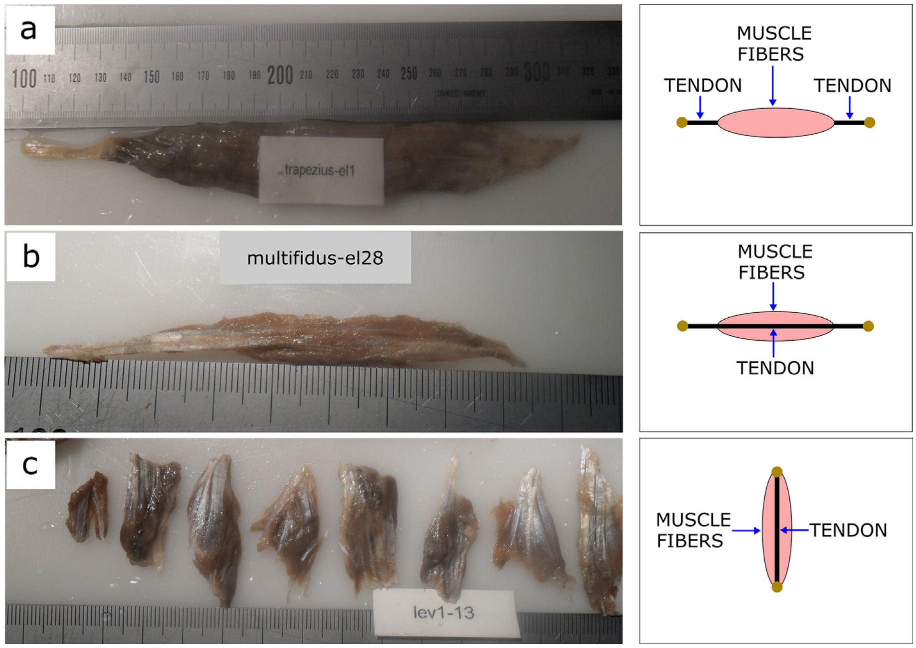

Fig. 2. Illustration of the muscle architecture measured in this study. (a) Proximal and distal tendons are joined by the muscle fibers (tendon-muscle-tendon architecture). (b) Muscle fibers run in parallel with the tendon, but do not span the total length of the tendon. (c) Muscle fibers run in parallel with the tendon and fully span.

Some muscles had intermediate tendons, connecting muscle bellies at either side of the muscle-tendon units, such as omohyoid (element 1), longissimus capitis (elements 1–3), and semispinalis capitis (elements 1–3). For these elements, we measured fiber lengths and masses and calculated physiological cross-sectional areas (PCSA) of the two bellies separately. We reported the largest PCSA of the two bellies. The masses, average fiber lengths, and average optimal-fiber lengths of the two bellies were summed, and the tendon length was calculated by subtracting total fiber length, multiplied by the cosine of the pennation angle, from the musculo-tendon length.

We discovered that some deeper muscles of the trunk such as the elements of the rotatores, levatores costarum, multifidus, and spinalis thoracis, differed in architecture as illustrated in Fig. 2. For example, the majority of the muscles reported in the present study had tendon-muscle-tendon architecture, (see Fig. 2a). On the other hand, some deeper muscles had their tendons running from their origin to insertion. In these muscles, fibers either spanned (in parallel with the tendon) the full length of the tendon (rotatores and levatores costarum, see Fig. 2c) or partially spanned (most elements of the multifidus and spinalis thoracis, see Fig. 2b). For these elements, we dissected tendon from the muscle and additionally calculated cross-sectional area (CSA, in cm^2) of the tendon by using Eq. (1),

$$CSA = \frac{m^t}{\rho^t \times \ell^t} \qquad (1)$$

where m^t is the mass, ρ^t is the density, and ℓ^t is the length of the tendon. We calculated average density of the tendon tissue (1.2041 g/cm^3) by dividing its mass by its volume measured using water dislocation method. Such muscle elements are indicated in Table 1 and Appendix A.3.

To reduce the study time, we performed measurements only between ribs 1 and 2, 5 and 6, and 9 and 10 for intercostales muscles. Similarly, we measured levatores costarum (longi) only at the upper and lower rib levels.

Finally, we graphically fitted wrapping surfaces–from the geometry of the spine and the point clouds which were collected over the structures that muscles wrap–in the AnyBody Modeling System™ version. 6.0.4 (AnyBody Technology A/S, Aalborg, Denmark). Depending on the shape of a surface, either a cylinder or an ellipsoid was fitted.

3. Results

The complete list of measured muscle elements is given in Table 1. In total, 225 muscle elements were measured for 39 muscles. For every element, we provided the coordinates of its attachments at origin and insertion and the morphological parameters: fiber length, sarcomere length, optimal fiber length, tendon length, pennation angle, mass, and physiological cross-sectional area (PCSA). Total muscle PCSAs ranged from 0.09 cm^2 for sternothyroid muscle to 14.27 cm^2 for trapezius muscle. Mean sarcomere lengths ranged from 2.10 μm for the sternothyroid muscle to 3.91 μm for semispinalis cervicis muscle. Mean optimal fiber lengths ranged from 0.6 cm for rectus capitis lateralis muscle to 14.7 cm for serratus anterior muscle. Mean tendon lengths ranged from 0.4 cm for the sternohyoid muscle to 16.4 cm for spinalis thoracis muscle. The coordinates of the via points, the mathematical definitions of the wrapping surfaces, and the architectural tendon parameters can be found in Appendix A.1–3, respectively as digital appendices. All the bone segments with re-constructed muscle lines-of-action were visualized in the AnyBody Modeling System™ ver. 6.0.4 (AnyBody Technology A/S, Aalborg, Denmark) and are depicted in Fig. 3.

4. Discussion

The aim of the present study was to obtain a complete and coherent musculo-skeletal dataset for modeling the thoracic and cervical regions of the human spine. For this purpose, we dissected several muscles from a single spine, measured the positions of their attachments at the bones, and obtained three-dimensional geometry of the bones (in the form of STL files). We chose to divide the muscles into a number of muscle-tendon elements to represent their function better in computer models. For every muscle element, we additionally measured the morphological parameters consisting of the fiber length, tendon length, sarcomere length, optimal fiber length, pennation angle, mass, and PCSA. These architectural parameters will enable better simulation of the muscle mechanics and hence will improve the muscle and joint force estimations in such models (Zajac, 1989; Vasavada et al., 1998; Thelen, 2003). For example, Carbone et al. (2016) investigated the sensitivity of their gait model against potential errors in morphological parameters for several muscles. They reported tendon slack length to be the most sensitive parameter, subsequently followed by maximal isometric muscle force, optimal muscle fiber length, and nominal pennation angle.

Morphological parameters of the neck muscles measured in this study are compared with similar anatomical studies in Table 2. The PCSAs of the individual elements of a muscle were summed, and a mean value of their optimal fiber lengths was calculated for comparison. PCSAs measured in this study fit well with the range of

Table 1
Per muscle element: element number (#), fiber length (ℓ^f), sarcomere length (ℓ^s), optimal fiber length (ℓ^f_o), tendon length (ℓ^t), pennation angle (α), physiological cross-sectional area (PCSA), and the coordinates of the attachments at the origin and insertion with respect to the global reference frame defined by the CT scanner.[a,d,e,f]

Muscle	#	ℓ^f (mm)	ℓ^s (μm)	ℓ^f_o (mm)	ℓ^t (mm)	α (deg)	Mass (g)	PCSA (cm^2)	Origin (bone)	Form	Position (m)			Insertion (bone)	Form	Position (m)		
											x	y	z			x	y	z
Iliocostalis cervicis[h]	1	57.7	3.39	45.9	106.3	0	0.65	0.13	R5	Point	−0.0603	−0.0682	1.0304	C5	Point	0.0024	−0.1809	1.1259
Iliocostalis cervicis[h]	2	57.7	3.39	45.9	75.3	0	0.65	0.13	R4	Point	−0.0513	−0.0876	1.0648	C5	Point	0.0024	−0.1809	1.1259
Iliocostalis cervicis[h]	3	57.7	3.39	45.9	54.3	0	0.65	0.13	R3	Point	−0.0466	−0.1007	1.0741	C5	Point	0.0024	−0.1809	1.1259
Iliocostalis thoracis[h]	1	147.5	2.81	141.6	59.0	0	2.85	0.19	R11	Point	−0.0659	−0.0501	0.8636	R5	Point	−0.0665	−0.0710	1.0394
Iliocostalis thoracis[h]	2	147.5	2.81	141.6	88.5	0	2.85	0.19	R10	Point	−0.0668	−0.0514	0.8931	R4	Point	−0.0544	−0.0864	1.0631
Iliocostalis thoracis[h]	3	147.5	2.81	141.6	80.0	0	2.85	0.19	R9	Point	−0.0684	−0.0481	0.9254	R3	Point	−0.0483	−0.1094	1.0810
Intercostales externi	1	11.8	3.02	10.6	6.7	0	0.13	0.12	R2	Line	−0.0288	−0.2262	1.0112	R1	Line	−0.0309	−0.2148	1.0261
Intercostales externi	2	13.3	3.02	11.9	14.7	0	2.50	1.99	R2	Line	−0.0738	−0.1890	1.0319	R1	Line	−0.0602	−0.1813	1.0502
Intercostales externi	3	13.5	3.02	12.1	15.5	0	2.92	2.29	R2	Line	−0.0679	−0.1377	1.0770	R1	Line	−0.0533	−0.1524	1.0840
Intercostales externi	4	20.3	3.02	18.1	15.8	0	1.46	0.76	R6	Line	−0.1206	−0.1842	0.9117	R5	Line	−0.1121	−0.1951	0.9263
Intercostales externi	5	10.8	3.02	9.7	15.2	0	2.70	2.64	R6	Line	−0.0981	−0.0796	0.9941	R5	Line	−0.0994	−0.0854	1.0003
Intercostales externi	6	15.7	3.02	14.0	10.3	0	3.01	2.03	R10	Line	−0.0972	−0.0675	0.8819	R9	Line	−0.1060	−0.0760	0.8907
Intercostales interni	1	7.5	2.36	8.6	16.5	0	0.96	1.06	R2	Line	−0.0709	−0.1949	1.0282	R1	Line	−0.0546	−0.1956	1.0430
Intercostales interni	2	13.7	2.36	15.7	9.3	0	1.83	1.11	R6	Line	−0.1149	−0.1974	0.9060	R5	Line	−0.1073	−0.2055	0.9221
Intercostales interni	3	13.7	2.36	15.7	9.3	0	0.77	0.47	R6	Line	−0.0978	−0.0816	0.9941	R5	Line	−0.1027	−0.0895	0.9941
Intercostales interni	4	20.6	2.36	23.6	3.4	0	4.31	1.73	R10	Line	−0.1218	−0.1489	0.7829	R9	Line	−0.1221	−0.1609	0.8070
Intercostales interni	5	14.6	2.36	16.8	8.9	0	0.68	0.38	R10	Line	−0.0933	−0.0638	0.8878	R9	Line	−0.1019	−0.0748	0.8959
Levator scapulae	1	127.3	3.04	113.1	31.7	0	4.62	0.39	C4	Point	−0.0003	−0.1894	1.1401	Scapula	Surface	−0.0533	−0.1029	1.1003
Levator scapulae	2	126.5	3.04	112.4	16.0	0	1.83	0.15	C3	Point	0.0029	−0.1931	1.1540	Scapula	Surface	−0.0533	−0.1029	1.1003
Levator scapulae	3	118.8	3.04	105.5	20.3	0	5.11	0.46	C2	Point	0.0038	−0.1948	1.1641	Scapula	Surface	−0.0533	−0.1029	1.1003
Levator scapulae	4	145.3	3.04	129.1	37.8	0	13.48	0.99	C1	Point	−0.0080	−0.1883	1.1882	Scapula	Surface	−0.0533	−0.1029	1.1003
Levatores costarum[c]	1	28.0	2.96	25.6	28.0	0	0.10	0.04	T2	Point	−0.0251	−0.1221	1.0961	R3	Point	−0.0436	−0.1076	1.0827
Levatores costarum[c,f]	2	49.0	2.96	44.7	49.0	0	0.14	0.03	T2	Point	−0.0251	−0.1221	1.0961	R4	Point	−0.0523	−0.0892	1.0648
Levatores costarum[c]	3	29.0	2.96	26.5	29.0	0	0.12	0.04	T3	Point	−0.0277	−0.1061	1.0797	R4	Point	−0.0468	−0.0876	1.0648
Levatores costarum[c]	4	29.0	2.96	26.5	29.0	0	0.24	0.09	T4	Point	−0.0308	−0.0897	1.0597	R5	Point	−0.0523	−0.0741	1.0447
Levatores costarum[c]	5	26.0	2.96	23.7	26.0	0	0.06	0.02	T5	Point	−0.0342	−0.0749	1.0368	R6	Point	−0.0534	−0.0630	1.0220
Levatores costarum[c]	6	33.0	2.96	30.1	33.0	0	0.12	0.04	T6	Point	−0.0345	−0.0619	1.0151	R7	Point	−0.0582	−0.0539	0.9968
Levatores costarum[c]	7	39.0	2.96	35.6	39.0	0	0.08	0.02	T7	Point	−0.0340	−0.0537	0.9880	R8	Point	−0.0603	−0.0471	0.9689
Levatores costarum[c]	8	35.0	2.96	32.0	35.0	0	0.12	0.04	T8	Point	−0.0347	−0.0487	0.9636	R9	Point	−0.0551	−0.0440	0.9406
Levatores costarum[c]	9	44.0	2.96	40.2	44.0	0	0.18	0.04	T9	Point	−0.0353	−0.0466	0.9320	R10	Point	−0.0616	−0.0461	0.9088
Levatores costarum[c,f]	10	59.0	2.96	53.9	59.0	0	0.85	0.15	T9	Point	−0.0353	−0.0466	0.9320	R11	Point	−0.0462	−0.0527	0.8772
Levatores costarum[c]	11	42.0	2.96	38.3	42.0	0	0.46	0.11	T10	Point	−0.0290	−0.0503	0.9056	R11	Point	−0.0462	−0.0527	0.8772
Levatores costarum[c,f]	12	72.0	2.96	65.7	72.0	0	0.14	0.02	T10	Point	−0.0290	−0.0503	0.9056	R12	Point	−0.0383	−0.0685	0.8488
Levatores costarum[c]	13	40.0	2.96	36.5	40.0	0	0.30	0.08	T11	Point	−0.0288	−0.0553	0.8777	R12	Point	−0.0383	−0.0685	0.8488
Longissimus capitis	1	115.0	2.81	110.4	120.0	0	0.85	0.09	T5	Point	−0.0295	−0.0729	1.0354	Skull	Line	−0.0244	−0.1746	1.2005
Longissimus capitis	2	115.0	2.81	110.4	102.0	0	0.85	0.09	T4	Point	−0.0267	−0.0883	1.0592	Skull	Line	−0.0244	−0.1746	1.2005
Longissimus capitis	3	115.0	2.81	110.4	96.0	0	0.85	0.09	T3	Point	−0.0230	−0.1039	1.0790	Skull	Line	−0.0244	−0.1746	1.2005
Longissimus capitis	4	39.5	2.81	37.9	51.5	0	0.34	0.08	C7	Point	−0.0129	−0.1646	1.1168	Skull	Line	−0.0244	−0.1746	1.2005
Longissimus capitis	5	39.5	2.81	37.9	43.5	0	0.34	0.08	C5	Point	−0.0003	−0.1818	1.1262	Skull	Line	−0.0244	−0.1746	1.2005
Longissimus capitis	6	39.5	2.81	37.9	40.0	0	0.34	0.08	C4	Point	0.0007	−0.1914	1.1417	Skull	Line	−0.0244	−0.1746	1.2005
Longissimus capitis	7	39.5	2.81	37.9	36.7	14	0.34	0.08	C3	Point	0.0045	−0.1929	1.1550	Skull	Line	−0.0244	−0.1746	1.2005
Longissimus cervicis	1	45.5	3.70	33.2	0.5	0	0.68	0.19	T1	Point	−0.0222	−0.1453	1.1100	C5	Point	−0.0003	−0.1818	1.1262
Longissimus cervicis	2	45.5	3.70	33.2	16.0	0	0.68	0.19	T2	Point	−0.0209	−0.1211	1.0978	C4	Point	0.0007	−0.1914	1.1417
Longissimus cervicis	3	45.5	3.70	33.2	46.5	0	0.68	0.19	T3	Point	−0.0150	−0.1108	1.0779	C3	Point	0.0045	−0.1929	1.1550
Longissimus cervicis	4	45.5	3.70	33.2	71.5	0	0.68	0.19	T5	Point	−0.0336	−0.0752	1.0346	C7	Point	−0.0129	−0.1646	1.1168
Longissimus cervicis	5	36.8	3.70	26.8	118.3	0	0.82	0.29	T6	Point	−0.0320	−0.0618	1.0133	C6	Point	−0.0043	−0.1755	1.1207
Longissimus cervicis	6	42.3	3.70	30.9	93.7	0	0.95	0.29	T4	Point	−0.0279	−0.0896	1.0562	C5	Point	−0.0003	−0.1818	1.1262
Longus capitis	1	37.1	2.58	38.8	85.9	0	0.81	0.20	C6	Point	−0.0034	−0.1785	1.1090	Skull	Line	0.0280	−0.2000	1.2200

(*continued on next page*)

Table 1 (*continued*)

Muscle	#	ℓ^f (mm)	ℓ^s (μm)	ℓ_o^f (mm)	ℓ^t (mm)	α (deg)	Mass (g)	PCSA (cm^2)	Origin (bone)	Form	Position (m)			Insertion (bone)	Form	Position (m)		
											x	y	z			x	y	z
Longus capitis	2	37.1	2.58	38.8	60.9	0	0.81	0.20	C5	Point	−0.0041	−0.1864	1.1250	Skull	Line	0.0280	−0.2000	1.2200
Longus capitis	3	25.5	2.58	26.6	52.5	0	0.77	0.27	C4	Point	0.0001	−0.1902	1.1383	Skull	Line	0.0280	−0.2000	1.2200
Longus capitis	4	27.0	2.58	28.2	26.0	0	0.66	0.22	C3	Point	0.0041	−0.1934	1.1503	Skull	Line	0.0280	−0.2000	1.2200
Multifidus	16	61.0	3.42	48.2	25.0	0	1.07	0.21	L4	Point	−0.0341	−0.0799	0.7411	T12	Point	−0.0066	−0.0485	0.8251
Multifidus	17	69.8	3.42	55.1	3.8	0	1.90	0.33	L3	Point	−0.0244	−0.0857	0.7673	T11	Point	−0.0062	−0.0424	0.8538
Multifidus	18	67.0	3.42	53.0	21.5	0	0.88	0.16	L2	Point	−0.0251	−0.0790	0.7874	T10	Point	−0.0076	−0.0376	0.8773
Multifidus[b]	19	56.5	3.42	44.7	95.0	0	0.26	0.06	L1	Point	−0.0248	−0.0706	0.8155	T9	Point	−0.0080	−0.0372	0.9070
Multifidus[b]	20	45.5	3.42	36.0	113.5	0	1.89	0.50	L1	Point	−0.0248	−0.0710	0.8152	T8	Point	−0.0068	−0.0395	0.9357
Multifidus[b]	21	82.0	3.42	64.8	139.0	0	0.20	0.03	L1	Point	−0.0248	−0.0710	0.8152	T7	Point	−0.0088	−0.0455	0.9590
Multifidus[c]	22	41.0	3.42	32.4	41.0	0	0.14	0.04	T12	Point	−0.0181	−0.0541	0.8560	T9	Point	−0.0083	−0.0387	0.8971
Multifidus[b]	23	35.0	3.42	27.7	53.0	0	0.19	0.06	T12	Point	−0.0185	−0.0554	0.8577	T9	Point	−0.0089	−0.0418	0.9042
Multifidus[b]	24	40.0	3.42	31.6	102.0	0	0.21	0.06	T12	Point	−0.0189	−0.0540	0.8561	T7	Point	−0.0080	−0.0386	0.9412
Multifidus[b]	25	32.0	3.42	25.3	79.0	0	0.07	0.03	T12	Point	−0.0188	−0.0564	0.8503	T6	Point	−0.0100	−0.0421	0.9702
Multifidus[b]	26	38.0	3.42	30.0	47.0	0	0.03	0.01	T11	Point	−0.0215	−0.0512	0.8836	T8	Point	−0.0091	−0.0387	0.9231
Multifidus[b]	27	22.0	3.42	17.4	57.0	0	0.07	0.04	T11	Point	−0.0247	−0.0516	0.8826	T7	Point	−0.0077	−0.0387	0.9405
Multifidus[b]	28	37.0	3.42	29.2	84.5	0	0.44	0.14	T11	Point	−0.0247	−0.0516	0.8826	T6	Point	−0.0103	−0.0418	0.9719
Multifidus[b]	29	22.0	3.42	17.4	39.5	0	0.38	0.21	T10	Point	−0.0204	−0.0523	0.9080	T7	Point	−0.0091	−0.0435	0.9529
Multifidus[b]	30	43.0	3.42	34.0	61.5	0	0.11	0.03	T10	Point	−0.0214	−0.0516	0.9142	T6	Point	−0.0101	−0.0457	0.9805
Multifidus[c]	31	35.5	3.42	28.1	35.5	0	0.04	0.01	T10	Point	−0.0243	−0.0517	0.9157	T7	Point	−0.0088	−0.0474	0.9551
Multifidus[b]	32	19.0	3.42	15.0	47.0	0	0.01	0.01	T9	Point	−0.0299	−0.0464	0.9274	T6	Point	−0.0077	−0.0426	0.9686
Multifidus[b]	33	39.0	3.42	30.8	66.0	0	0.25	0.08	T9	Point	−0.0289	−0.0445	0.9309	T6	Point	−0.0080	−0.0552	0.9997
Multifidus[b]	34	16.0	3.42	12.6	65.5	0	0.01	0.01	T9	Point	−0.0289	−0.0445	0.9309	T5	Point	−0.0077	−0.0670	1.0270
Multifidus[b]	35	36.0	3.42	28.5	93.0	0	0.12	0.04	T9	Point	−0.0281	−0.0457	0.9358	T4	Point	−0.0122	−0.0632	1.0343
Multifidus[b]	36	29.0	3.42	22.9	70.0	0	0.24	0.10	T9	Point	−0.0253	−0.0489	0.9399	T5	Point	−0.0093	−0.0511	1.0013
Multifidus[b]	37	21.0	3.42	16.6	37.0	0	0.05	0.03	T9	Point	−0.0256	−0.0516	0.9417	T6	Point	−0.0105	−0.0494	0.9792
Multifidus[b]	38	29.0	3.42	22.9	44.0	0	0.24	0.10	T8	Point	−0.0249	−0.0526	0.9651	T5	Point	−0.0093	−0.0511	1.0013
Multifidus[b]	39	25.0	3.42	19.8	44.0	0	0.11	0.05	T8	Point	−0.0249	−0.0528	0.9662	T5	Point	−0.0103	−0.0553	1.0109
Multifidus[b]	40	74.0	3.42	58.5	105.0	0	0.40	0.06	T8	Point	−0.0306	−0.0496	0.9595	T3	Point	−0.0066	−0.0787	1.0599
Multifidus[b]	41	34.0	3.42	26.9	67.0	0	0.38	0.13	T8	Point	−0.0282	−0.0545	0.9689	T4	Point	−0.0123	−0.0638	1.0357
Multifidus[b]	42	27.0	3.42	21.3	44.0	0	0.08	0.04	T8	Point	−0.0263	−0.0561	0.9688	T5	Point	−0.0101	−0.0599	1.0088
Multifidus[b]	43	53.0	3.42	41.9	85.0	0	0.23	0.05	T7	Point	−0.0266	−0.0562	0.9861	T3	Point	−0.0061	−0.0817	1.0608
Multifidus[b]	44	45.0	3.42	35.6	100.5	0	0.48	0.13	T7	Point	−0.0301	−0.0529	0.9880	T2	Point	−0.0024	−0.0935	1.0828
Multifidus[b]	45	35.0	3.42	27.7	48.5	0	0.11	0.04	T7	Point	−0.0240	−0.0651	0.9931	T4	Point	−0.0083	−0.0749	1.0375
Multifidus[b]	46	43.0	3.42	34.0	76.5	0	0.20	0.06	T7	Point	−0.0296	−0.0616	0.9938	T3	Point	−0.0054	−0.0826	1.0601
Multifidus[b]	47	43.0	3.42	34.0	79.0	0	0.13	0.03	T6	Point	−0.0296	−0.0635	1.0182	T2	Point	−0.0024	−0.0935	1.0828
Multifidus[b]	48	43.0	3.42	34.0	101.0	0	0.13	0.03	T6	Point	−0.0296	−0.0635	1.0182	T1	Point	0.0002	−0.1071	1.0984
Multifidus[b]	49	35.0	3.42	27.7	76.5	0	0.18	0.06	T6	Point	−0.0279	−0.0690	1.0212	T2	Point	−0.0011	−0.0981	1.0818
Multifidus[b]	50	22.0	3.42	17.4	49.0	0	0.09	0.05	T6	Point	−0.0280	−0.0701	1.0210	T3	Point	−0.0041	−0.0912	1.0588
Multifidus[b]	51	34.5	3.42	27.3	45.0	0	0.26	0.09	T5	Point	−0.0330	−0.0775	1.0419	T2	Point	−0.0005	−0.1070	1.0799
Multifidus[b]	52	34.5	3.42	27.3	61.0	0	0.26	0.09	T5	Point	−0.0330	−0.0775	1.0419	T1	Point	0.0018	−0.1128	1.0971
Multifidus[c]	53	37.5	3.42	29.6	37.5	0	0.10	0.03	T4	Point	−0.0211	−0.0980	1.0647	T1	Point	0.0046	−0.1158	1.0944
Multifidus[b]	54	51.0	3.42	40.3	66.0	0	0.81	0.19	T4	Point	−0.0229	−0.0962	1.0662	C7	Point	0.0132	−0.1304	1.1113
Multifidus[b]	55	22.0	3.42	17.4	43.0	0	0.02	0.01	T3	Point	−0.0200	−0.1145	1.0829	C7	Point	0.0130	−0.1295	1.1119
Multifidus[c]	56	47.0	3.42	37.1	47.0	0	0.04	0.01	T3	Point	−0.0201	−0.1156	1.0812	C7	Point	0.0108	−0.1364	1.1100
Multifidus[b]	57	20.0	3.42	15.8	39.5	0	0.19	0.11	T2	Point	−0.0193	−0.1322	1.0998	C6	Point	0.0181	−0.1433	1.1252
Multifidus[c]	58	34.0	3.42	26.9	34.0	0	0.61	0.21	T1	Point	−0.0133	−0.1481	1.1120	C6	Point	0.0179	−0.1461	1.1248
Multifidus[c]	59	48.0	3.42	37.9	48.0	0	0.58	0.14	T1	Point	−0.0133	−0.1481	1.1120	C4	Point	0.0164	−0.1528	1.1379
Multifidus[b]	60	31.0	3.42	24.5	44.5	0	0.97	0.37	T1	Point	−0.0133	−0.1481	1.1120	C4	Point	0.0164	−0.1528	1.1379
Multifidus[b]	61	23.0	3.42	18.2	33.0	0	0.65	0.34	C7	Point	−0.0018	−0.1617	1.1191	C5	Point	0.0178	−0.1528	1.1357
Multifidus[c]	62	39.0	3.42	30.8	39.0	0	0.39	0.12	C7	Point	−0.0099	−0.1659	1.1189	C4	Point	0.0196	−0.1551	1.1401
Multifidus[c]	63	36.5	3.42	28.8	36.5	0	0.35	0.11	C5	Point	−0.0022	−0.1679	1.1293	C3	Point	0.0233	−0.1618	1.1546
Multifidus[c]	64	39.0	3.42	30.8	39.0	0	0.28	0.09	C4	Point	0.0000	−0.1771	1.1401	C2	Point	0.0207	−0.1620	1.1651
Obliquus capitis inferior	1	35.3	2.69	35.3	12.8	0	5.40	1.45	C2	Surface	0.0226	−0.1641	1.1702	C1	Surface	−0.0034	−0.1893	1.1850

Table 1 (*continued*)

Muscle	#	ℓ^f (mm)	ℓ^s (μm)	ℓ_o^f (mm)	ℓ^t (mm)	α (deg)	Mass (g)	PCSA (cm^2)	Origin (bone)	Form	Position (m)			Insertion (bone)	Form	Position (m)		
											x	y	z			x	y	z
Obliquus capitis superior	1	21.3	3.16	18.2	33.8	0	0.63	0.33	C1	Surface	−0.0074	−0.1900	1.1858	Skull	Surface	−0.0097	−0.1594	1.1951
Omohyoid[h]	1	117.8	2.45	129.6	51.2	0	3.26	0.24	Scapula	Line	−0.0829	−0.1200	1.0966	Hyoid	Line	0.0034	−0.2220	1.1412
Omohyoid	2	50.5	2.45	55.6	21.0	0	0.38	0.06	Scapula	Point	−0.0896	−0.1356	1.1008	Clavicle	Point	−0.0476	−0.1934	1.0781
Rectus capitis anterior	1	9.5	2.63	9.7	13.5	0	0.21	0.20	C1	Line	0.0038	−0.1941	1.1957	Skull	Line	0.0191	−0.1944	1.2059
Rectus capitis lateralis[g]	1	6.3	2.63	6.4	11.8	0	0.07	0.10	C1	Line	−0.0063	−0.1950	1.1898	Skull	Line	−0.0218	−0.1887	1.2020
Rectus capitis posterior major	1	29.0	2.83	27.7	10.0	0	3.04	1.04	C2	Point	0.0272	−0.1543	1.1661	Skull	Surface	0.0036	−0.1479	1.1900
Rectus capitis posterior minor	1	14.5	2.99	13.1	15.5	0	0.42	0.30	C1	Point	0.0272	−0.1642	1.1821	Skull	Line	0.0093	−0.1479	1.1891
Rhomboideus major	1	122.3	3.19	103.5	63.7	0	10.28	0.94	T3	Line	−0.0025	−0.0779	1.0673	Scapula	Line	−0.0958	−0.0481	0.9980
Rhomboideus major	2	115.2	3.19	97.5	60.8	0	23.16	2.25	T1	Line	0.0073	−0.1132	1.1111	Scapula	Line	−0.0807	−0.0496	1.0340
Rhomboideus minor	1	105.5	3.19	89.3	64.5	0	31.68	3.35	C6	Line	0.0165	−0.1214	1.1288	Scapula	Line	−0.0571	−0.0691	1.0837
Rotatores[c]	1	30.0	3.03	26.7	30.0	0	0.14	0.05	T12	Point	−0.0181	−0.0541	0.8560	T10	Point	−0.0076	−0.0486	0.8842
Rotatores[c]	2	30.0	3.03	26.7	30.0	0	0.19	0.07	T12	Point	−0.0185	−0.0554	0.8577	T10	Point	−0.0111	−0.0543	0.8877
Rotatores[c]	3	26.0	3.03	23.2	26.0	0	0.03	0.01	T11	Point	−0.0215	−0.0512	0.8836	T9	Point	−0.0088	−0.0446	0.9060
Rotatores[c]	4	23.0	3.03	20.5	23.0	0	0.10	0.05	T11	Point	−0.0193	−0.0543	0.8838	T9	Point	−0.0071	−0.0529	0.9093
Rotatores[c]	5	18.0	3.03	16.0	18.0	0	0.01	0.01	T10	Point	−0.0286	−0.0532	0.9145	T9	Point	−0.0081	−0.0507	0.9221
Rotatores[c]	6	20.0	3.03	17.8	20.0	0	0.02	0.01	T10	Point	−0.0199	−0.0541	0.9133	T8	Point	−0.0085	−0.0492	0.9339
Rotatores[c]	7	26.0	3.03	23.2	26.0	0	0.19	0.08	T9	Point	−0.0231	−0.0506	0.9366	T7	Point	−0.0091	−0.0521	0.9601
Rotatores[c]	8	13.0	3.03	11.6	13.0	0	0.02	0.02	T9	Point	−0.0201	−0.0533	0.9351	T8	Point	−0.0105	−0.0522	0.9384
Rotatores[c]	9	15.0	3.03	13.4	15.0	0	0.19	0.13	T9	Point	−0.0201	−0.0533	0.9351	T8	Point	−0.0140	−0.0552	0.9489
Rotatores[c]	10	8.0	3.03	7.1	8.0	0	0.03	0.03	T8	Point	−0.0206	−0.0603	0.9670	T7	Point	−0.0127	−0.0561	0.9668
Rotatores[c]	11	24.0	3.03	21.4	24.0	0	0.03	0.01	T8	Point	−0.0206	−0.0603	0.9670	T6	Point	−0.0102	−0.0583	0.9879
Rotatores[c]	12	8.0	3.03	7.1	8.0	0	0.06	0.07	T7	Point	−0.0205	−0.0617	0.9888	T6	Point	−0.0142	−0.0632	0.9940
Rotatores[c]	13	26.5	3.03	23.6	26.5	0	0.06	0.02	T7	Point	−0.0255	−0.0660	0.9931	T5	Point	−0.0115	−0.0698	1.0166
Rotatores[c]	14	9.0	3.03	8.0	9.0	0	0.03	0.04	T6	Point	−0.0242	−0.0711	1.0194	T5	Point	−0.0143	−0.0725	1.0190
Rotatores[c]	15	38.0	3.03	33.9	38.0	0	0.03	0.01	T6	Point	−0.0199	−0.0719	1.0163	T4	Point	−0.0080	−0.0826	1.0420
Rotatores[c]	16	9.0	3.03	8.0	9.0	0	0.03	0.04	T5	Point	−0.0189	−0.0846	1.0403	T4	Point	−0.0103	−0.0849	1.0430
Rotatores[c]	17	27.5	3.03	24.5	27.5	0	0.03	0.01	T5	Point	−0.0244	−0.0845	1.0420	T3	Point	−0.0062	−0.0986	1.0600
Rotatores[c]	18	7.0	3.03	6.2	7.0	0	0.05	0.07	T4	Point	−0.0154	−0.0984	1.0601	T3	Point	−0.0082	−0.1006	1.0608
Rotatores[c]	19	26.5	3.03	23.6	26.5	0	0.05	0.02	T4	Point	−0.0189	−0.0991	1.0629	T2	Point	−0.0004	−0.1098	1.0780
Rotatores[c]	20	31.5	3.03	28.1	31.5	0	0.04	0.01	T3	Point	−0.0218	−0.1071	1.0832	T1	Point	0.0034	−0.1218	1.0950
Rotatores[c]	21	27.0	3.03	24.1	27.0	0	0.23	0.09	T3	Point	−0.0131	−0.1118	1.0760	T1	Point	0.0034	−0.1218	1.0950
Rotatores[c]	22	19.0	3.03	16.9	19.0	0	0.07	0.04	T3	Point	−0.0163	−0.1145	1.0801	T1	Point	0.0026	−0.1257	1.0943
Rotatores[c]	23	30.5	3.03	27.2	30.5	0	0.24	0.08	T2	Point	−0.0161	−0.1304	1.0979	C7	Point	0.0081	−0.1422	1.1106
Rotatores[c]	24	30.5	3.03	27.2	30.5	0	0.24	0.08	T2	Point	−0.0142	−0.1276	1.0951	C7	Point	0.0091	−0.1402	1.1083
Rotatores[c]	25	21.0	3.03	18.7	21.0	0	0.13	0.07	T2	Point	−0.0142	−0.1276	1.0951	T1	Point	−0.0016	−0.1319	1.0961
Rotatores[c]	26	27.5	3.03	24.5	27.5	0	0.15	0.06	T1	Point	−0.0115	−0.1442	1.1098	C6	Point	0.0180	−0.1423	1.1251
Scalenus anterior	1	25.7	2.37	29.2	34.3	0	0.89	0.29	C7	Point	−0.0120	−0.1671	1.1044	R1	Surface	−0.0522	−0.1747	1.0660
Scalenus anterior	2	25.7	2.37	29.2	44.3	0	0.89	0.29	C6	Point	−0.0028	−0.1784	1.1099	R1	Surface	−0.0522	−0.1747	1.0660
Scalenus anterior	3	25.7	2.37	29.2	41.3	0	0.89	0.29	C5	Point	−0.0022	−0.1829	1.1234	R1	Surface	−0.0522	−0.1747	1.0660
Scalenus medius	1	22.3	2.65	22.7	44.8	0	2.38	0.99	C6	Point	−0.0068	−0.1759	1.1191	R1	Surface	−0.0561	−0.1608	1.0788
Scalenus medius	2	39.5	2.65	40.3	30.5	0	0.76	0.18	C5	Point	−0.0043	−0.1859	1.1250	R1	Surface	−0.0561	−0.1608	1.0788
Scalenus medius	3	50.0	2.65	51.0	34.0	0	2.38	0.44	C4	Point	−0.0004	−0.1901	1.1400	R1	Surface	−0.0561	−0.1608	1.0788
Scalenus medius	4	40.3	2.65	41.1	56.8	0	0.90	0.21	C3	Point	0.0026	−0.1937	1.1537	R1	Surface	−0.0561	−0.1608	1.0788
Scalenus medius	5	100.0	2.65	102.1	19.0	0	0.90	0.08	C2	Point	0.0037	−0.1951	1.1648	R1	Surface	−0.0561	−0.1608	1.0788
Scalenus medius	6	69.0	2.65	70.4	57.0	0	2.38	0.32	C1	Point	−0.0033	−0.1974	1.1852	R1	Surface	−0.0561	−0.1608	1.0788
Scalenus posterior	1	47.4	2.48	51.6	38.6	0	2.29	0.42	C3	Point	0.0037	−0.1929	1.1546	R1	Line	−0.0525	−0.1523	1.0858
Semispinalis capitis	1	142.5	3.06	125.6	80.7	10	1.55	0.16	T6	Point	−0.0318	−0.0626	1.0126	Skull	Surface	0.0179	−0.1228	1.1930
Semispinalis capitis	2	142.5	3.06	125.6	55.2	10	1.55	0.16	T5	Point	−0.0284	−0.0743	1.0401	Skull	Surface	0.0179	−0.1228	1.1930

(*continued on next page*)

Table 1 (*continued*)

Muscle	#	ℓ^f (mm)	ℓ^s (μm)	ℓ^f_o (mm)	ℓ^t (mm)	α (deg)	Mass (g)	PCSA (cm^2)	Origin (bone)	Form	Position (m)			Insertion (bone)	Form	Position (m)		
											x	y	z			x	y	z
Semispinalis capitis	3	101.8	3.06	89.7	65.7	0	3.01	0.33	T4	Point	−0.0267	−0.0883	1.0592	Skull	Surface	0.0179	−0.1228	1.1930
Semispinalis capitis	4	96.0	3.06	84.6	34.5	0	2.35	0.26	T3	Point	−0.0240	−0.1041	1.0791	Skull	Surface	0.0179	−0.1228	1.1930
Semispinalis capitis	5	82.3	3.06	72.5	27.7	0	2.54	0.33	T2	Point	−0.0231	−0.1216	1.0978	Skull	Surface	0.0179	−0.1228	1.1930
Semispinalis capitis	6	82.3	3.06	72.5	17.7	0	2.54	0.33	T1	Line	−0.0179	−0.1457	1.1126	Skull	Surface	0.0179	−0.1228	1.1930
Semispinalis capitis	7	48.8	3.06	43.0	39.8	0	1.97	0.43	C7	Point	−0.0131	−0.1638	1.1160	Skull	Surface	−0.0014	−0.1333	1.1939
Semispinalis capitis	8	48.8	3.06	43.0	37.3	0	1.97	0.43	C6	Point	−0.0046	−0.1745	1.1192	Skull	Surface	−0.0014	−0.1333	1.1939
Semispinalis capitis	9	48.8	3.06	43.0	31.3	0	1.97	0.43	C5	Point	0.0015	−0.1841	1.1322	Skull	Surface	−0.0014	−0.1333	1.1939
Semispinalis capitis	10	42.0	3.06	37.0	39.0	0	0.80	0.20	C4	Point	0.0015	−0.1886	1.1408	Skull	Surface	−0.0014	−0.1333	1.1939
Semispinalis cervicis	1	69.5	3.91	48.0	42.0	0	1.71	0.34	T5	Point	−0.0279	−0.0766	1.0436	C6	Point	0.0172	−0.1391	1.1273
Semispinalis cervicis	2	73.3	3.91	50.7	61.7	0	0.81	0.15	T5	Point	−0.0279	−0.0766	1.0436	C4	Point	0.0188	−0.1520	1.1391
Semispinalis cervicis	3	61.0	3.91	42.1	32.0	0	2.19	0.49	T4	Point	−0.0269	−0.0882	1.0598	C6	Point	0.0172	−0.1391	1.1273
Semispinalis cervicis	4	41.5	3.91	28.7	62.5	0	0.20	0.07	T4	Point	−0.0269	−0.0882	1.0598	C4	Point	0.0188	−0.1520	1.1391
Semispinalis cervicis	5	63.0	3.91	43.5	48.0	0	1.32	0.29	T4	Point	−0.0269	−0.0882	1.0598	C4	Point	0.0188	−0.1520	1.1391
Semispinalis cervicis	6	67.5	3.91	46.6	65.5	0	0.42	0.09	T4	Point	−0.0269	−0.0882	1.0598	C2	Point	0.0232	−0.1576	1.1575
Semispinalis cervicis	7	52.0	3.91	35.9	20.5	0	0.28	0.07	T3	Point	−0.0203	−0.1072	1.0822	C5	Point	0.0153	−0.1457	1.1330
Semispinalis cervicis	8	46.5	3.91	32.1	40.5	0	0.28	0.08	T3	Point	−0.0203	−0.1072	1.0822	C2	Point	0.0232	−0.1576	1.1575
Semispinalis cervicis	9	46.5	3.91	32.1	13.5	0	0.59	0.17	T2	Point	−0.0181	−0.1262	1.0990	C4	Point	0.0188	−0.1520	1.1391
Semispinalis cervicis	10	49.5	3.91	34.2	13.0	0	1.13	0.31	T1	Point	−0.0161	−0.1444	1.1124	C2	Point	0.0232	−0.1576	1.1575
Semispinalis thoracis[h]	1	55.4	3.80	39.3	96.6	0	0.68	0.16	T9	Point	−0.0312	−0.0458	0.9278	T2	Point	−0.0028	−0.0934	1.0840
Semispinalis thoracis[h]	2	55.4	3.80	39.3	100.6	0	0.68	0.16	T8	Point	−0.0328	−0.0477	0.9622	T1	Point	−0.0007	−0.1090	1.1030
Semispinalis thoracis[h]	3	55.4	3.80	39.3	84.6	0	0.68	0.16	T7	Point	−0.0317	−0.0537	0.9910	C7	Point	0.0106	−0.1200	1.1163
Semispinalis thoracis[h]	4	55.4	3.80	39.3	89.6	0	0.68	0.16	T6	Point	−0.0319	−0.0613	1.0143	C6	Point	0.0169	−0.1351	1.1316
Serratus anterior[i]	1	143.2	2.40	161.3	19.3	0	7.91	0.46	R8	Line	−0.1464	−0.1477	0.8547	Scapula	Line	−0.1062	−0.0588	0.9743
Serratus anterior[i]	2	149.0	2.40	167.9	24.0	0	15.41	0.87	R7	Line	−0.1426	−0.1679	0.8687	Scapula	Line	−0.1133	−0.0672	0.9776
Serratus anterior[i]	3	176.2	2.40	198.5	13.8	0	15.97	0.76	R6	Line	−0.1221	−0.2017	0.8901	Scapula	Line	−0.1209	−0.0779	0.9856
Serratus anterior[i]	4	146.3	2.40	164.9	38.7	0	13.17	0.76	R5	Line	−0.1176	−0.2024	0.9201	Scapula	Line	−0.1043	−0.0559	0.9752
Serratus anterior[i]	5	137.8	2.40	155.2	25.3	0	7.92	0.48	R4	Line	−0.1129	−0.1958	0.9518	Scapula	Line	−0.0996	−0.0513	0.9892
Serratus anterior[i]	6	119.3	2.40	134.4	34.3	0	13.78	0.97	R3	Line	−0.1058	−0.1963	0.9737	Scapula	Line	−0.0967	−0.0489	0.9962
Serratus anterior[i]	7	86.7	2.40	97.7	38.3	0	20.71	2.01	R2	Line	−0.0929	−0.1685	1.0238	Scapula	Line	−0.0824	−0.0500	1.0297
Serratus anterior[i]	8	84.7	2.40	95.4	8.3	0	23.07	2.29	R1	Line	−0.0745	−0.1606	1.0580	Scapula	Line	−0.0495	−0.0913	1.1055
Serratus posterior superior[i]	1	39.5	3.59	29.7	77.5	0	0.83	0.26	T1	Line	0.0022	−0.1053	1.1033	R3	Line	−0.0597	−0.1020	1.0741
Serratus posterior superior[i]	2	40.8	3.59	30.6	81.3	0	2.13	0.66	C7	Line	0.0153	−0.1163	1.1192	R2	Line	−0.0553	−0.1274	1.0910
Serratus posterior superior[i]	3	31.8	3.59	23.9	47.2	0	1.79	0.71	C6	Line	0.0210	−0.1326	1.1299	R1	Line	−0.0354	−0.1532	1.1018
Spinalis thoracis[b,h]	1	25.0	3.55	19.0	110.0	0	0.02	0.01	T12	Point	−0.0089	−0.0438	0.8282	T6	Point	−0.0102	−0.0410	0.9749
Spinalis thoracis[b,h]	2	54.0	3.55	41.1	140.0	0	0.32	0.07	T12	Point	−0.0089	−0.0438	0.8282	T5	Point	−0.0093	−0.0494	1.0057
Spinalis thoracis[b,h]	3	41.3	3.55	31.4	186.0	0	0.53	0.16	L1	Point	−0.0075	−0.0458	0.8100	T4	Point	−0.0090	−0.0604	1.0316
Spinalis thoracis[b,h]	4	47.0	3.55	35.8	219.5	0	0.78	0.21	L1	Point	−0.0075	−0.0458	0.8100	T4	Point	−0.0093	−0.0690	1.0432
Spinalis thoracis[b,h]	5	53.0	3.55	40.3	224.0	0	1.02	0.24	L1	Point	−0.0075	−0.0458	0.8100	T3	Point	−0.0071	−0.0768	1.0600
Spinalis thoracis[b,h]	6	20.0	3.55	15.2	101.5	0	0.04	0.02	T12	Point	−0.0089	−0.0438	0.8282	T7	Point	−0.0072	−0.0390	0.9401
Splenius capitis	1	93.1	3.16	79.5	32.9	0	8.04	0.96	C7	Line	0.0146	−0.1246	1.1227	Skull	Line	−0.0290	−0.1798	1.2049
Splenius capitis	2	67.7	3.16	57.8	28.3	0	6.55	1.07	C4	Line	0.0222	−0.1377	1.1462	Skull	Line	−0.0273	−0.1531	1.2102
Splenius cervicis	1	77.5	3.55	58.9	79.5	0	2.89	0.46	T3	Line	−0.0022	−0.0863	1.0722	C3	Point	0.0029	−0.1931	1.1540
Splenius cervicis	2	83.0	3.55	63.1	75.0	0	5.17	0.77	T2	Line	0.0035	−0.1022	1.0921	C1	Point	−0.0024	−0.1959	1.1842
Sternocleidomastoid	1	126.7	2.94	116.3	48.8	0	13.76	1.12	Sternum	Surface	0.0016	−0.2165	1.0441	Skull	Surface	−0.0279	−0.1765	1.2033
Sternocleidomastoid	2	118.7	2.94	109.0	87.3	0	12.00	1.04	Sternum	Surface	−0.0054	−0.2181	1.0430	Skull	Line	−0.0301	−0.1580	1.2119
Sternocleidomastoid	3	80.0	2.94	73.0	61.0	0	10.30	1.33	Clavicle	Surface	−0.0318	−0.2050	1.0725	Skull	Line	−0.0279	−0.1765	1.2033
Sternocleidomastoid	4	112.8	2.94	103.6	55.2	0	3.15	0.29	Clavicle	Surface	−0.0437	−0.1999	1.0813	Skull	Line	−0.0192	−0.1351	1.2101
Sternohyoid	1	85.5	2.71	85.3	5.5	0	1.43	0.16	Sternum	Line	0.0014	−0.2014	1.0514	Hyoid	Line	0.0119	−0.2303	1.1417
Sternohyoid	2	79.0	2.71	78.8	3.0	0	1.40	0.17	Clavicle	Line	−0.0111	−0.1984	1.0609	Hyoid	Line	0.0057	−0.2261	1.1402

Table 1 (*continued*)

Muscle	#	ℓ^f (mm)	ℓ^s (μm)	ℓ^f_o (mm)	ℓ^t (mm)	α (deg)	Mass (g)	PCSA (cm^2)	Origin (bone)	Form	Position (m)			Insertion (bone)	Form	Position (m)		
											x	y	z			x	y	z
Sternothyroid	1	60.0	2.10	77.0	6.5	0	0.26	0.03	R1	Line	−0.0298	−0.1930	1.0520	Thyroid	Line	0.0032	−0.2047	1.1218
Sternothyroid	2	50.2	2.10	64.4	10.8	0	0.39	0.06	Sternum	Line	0.0014	−0.2014	1.0514	Thyroid	Line	0.0064	−0.2123	1.1155
Subclavious	1	36.0	2.30	42.3	54.0	0	1.51	0.34	R1	Surface	−0.0445	−0.1920	1.0522	Clavicle	Surface	−0.0856	−0.1735	1.1053
Subcostales	1	23.0	2.33	26.7	36.5	0	0.17	0.06	R11	Line	−0.0371	−0.0657	0.8831	R9	Line	−0.0706	−0.0523	0.9301
Subcostales	2	23.5	2.33	27.2	28.5	0	0.45	0.16	R10	Line	−0.0374	−0.0586	0.9180	R8	Line	−0.0680	−0.0554	0.9611
Subcostales	3	26.0	2.33	30.1	17.5	0	0.72	0.23	R9	Line	−0.0415	−0.0563	0.9480	R7	Line	−0.0579	−0.0600	0.9892
Subcostales	4	23.5	2.33	27.2	15.5	0	0.31	0.11	R8	Line	−0.0434	−0.0583	0.9741	R6	Line	−0.0505	−0.0691	1.0139
Subcostales	5	26.3	2.33	30.4	12.8	0	0.41	0.13	R7	Line	−0.0424	−0.0658	1.0000	R5	Line	−0.0544	−0.0800	1.0350
Subcostales	6	10.0	2.33	11.6	10.0	0	0.05	0.04	R6	Line	−0.0463	−0.0732	1.0201	R5	Line	−0.0501	−0.0820	1.0387
Subcostales	7	21.8	2.33	25.2	22.8	0	0.81	0.30	R5	Line	−0.0510	−0.0816	1.0382	R3	Line	−0.0572	−0.1105	1.0710
Subcostales	8	23.3	2.33	27.0	23.3	0	0.33	0.12	R4	Line	−0.0453	−0.0949	1.0580	R2	Line	−0.0504	−0.1322	1.0872
Thyrohyoid	1	24.8	2.46	27.1	4.3	0	0.95	0.33	Thyroid	Line	0.0038	−0.2060	1.1202	Hyoid	Line	0.0028	−0.2192	1.1416
Transversus thoracis	1	24.7	2.90	23.0	55.3	0	0.39	0.16	R2	Line	−0.0577	−0.2088	1.0158	Sternum	Line	−0.0126	−0.2298	0.9535
Transversus thoracis	2	25.8	2.90	24.0	36.3	0	0.38	0.15	R3	Line	−0.0632	−0.2248	0.9769	Sternum	Line	−0.0103	−0.2289	0.9431
Transversus thoracis	3	24.7	2.90	23.0	52.3	0	0.47	0.19	R4	Line	−0.0768	−0.2230	0.9498	Sternum	Line	−0.0027	−0.2276	0.9286
Transversus thoracis	4	25.3	2.90	23.5	34.3	0	0.38	0.15	R5	Line	−0.0600	−0.2350	0.9300	Sternum	Line	−0.0021	−0.2268	0.9171
Transversus thoracis	5	20.8	2.90	19.3	38.8	0	0.10	0.05	R5	Line	−0.0584	−0.2351	0.9104	Sternum	Line	0.0005	−0.2275	0.9049
Transversus thoracis	6	11.5	2.90	10.7	31.5	0	0.06	0.05	R6	Line	−0.0523	−0.2338	0.8819	Sternum	Line	−0.0090	−0.2334	0.8841
Trapezius[i]	1	115.4	2.86	109.0	100.6	0	10.37	0.90	T8	Line	−0.0074	−0.0342	0.9348	Scapula	Point	−0.0940	−0.0775	1.0940
Trapezius[i]	2	90.8	2.86	85.8	82.7	0	12.14	1.34	T6	Line	−0.0071	−0.0396	0.9825	Scapula	Point	−0.0940	−0.0775	1.0940
Trapezius[i]	3	76.2	2.86	71.9	40.8	0	6.80	0.89	T5	Line	−0.0081	−0.0543	1.0209	Scapula	Line	−0.0853	−0.0760	1.0902
Trapezius[i]	4	62.8	2.86	59.3	27.8	0	4.22	0.67	T4	Line	−0.0083	−0.0666	1.0537	Scapula	Point	−0.0689	−0.0748	1.0854
Trapezius[i]	5	60.8	2.86	57.4	33.8	0	3.85	0.63	T3	Line	−0.0043	−0.0756	1.0675	Scapula	Line	−0.0826	−0.0786	1.0895
Trapezius[i]	6	70.3	2.86	66.3	66.3	10	25.70	3.61	T2	Line	0.0003	−0.0940	1.0902	Scapula	Line	−0.1152	−0.0971	1.1049
Trapezius	7	83.7	2.86	79.0	81.1	10	28.29	3.33	C6	Line	0.0187	−0.1181	1.1285	Scapula	Line	−0.1309	−0.1223	1.1172
Trapezius	8	86.5	2.86	81.7	81.5	0	11.97	1.39	C3	Line	0.0252	−0.1340	1.1511	Clavicle	Line	−0.1172	−0.1457	1.1322
Trapezius	9	91.5	2.86	86.4	51.5	0	13.77	1.51	C2	Line	0.0248	−0.1322	1.1643	Clavicle	Line	−0.0856	−0.1606	1.1216

[a] Unless noted otherwise, muscle elements had tendon-muscle fiber-tendon architecture as illustrated in Fig. 2a.
[b] Muscle fibers partially spanned the length of the tendon (see Fig. 2b).
[c] Muscle fibers spanned the full length of the tendon (see Fig. 2c).
[d] Numbering the elements of the multifidus muscle starts from sixteen. The first fifteen elements belonged to the lumbar region of the spine and were described in our previous study (Bayoglu et al., 2017).
[e] We measured intercostales interni and intercostales externi muscles only at the following levels: between ribs 1 and 2, 5 and 6, and 9 and 10.
[f] We measured the levatores costarum longi only at the upper and lower rib levels.
[g] We could not get good samples for the sarcomere length measurements from the rectus capitis lateralis muscle. Therefore, we assumed a mean sarcomere length of 2.63 μm (calculated mean sarcomere length for the rectus capitis anterior muscle) for this muscle.
[h] The coordinates of the via points for the iliocostalis cervicis, iliocostalis thoracis, omohyoid, semispinalis thoracis, and spinalis thoracis muscles are given in Appendix A.1.
[i] The mathematical definitions of the wrapping surfaces for the trapezius, serratus anterior, and serratus posterior superior muscles are given in Appendix A.2.

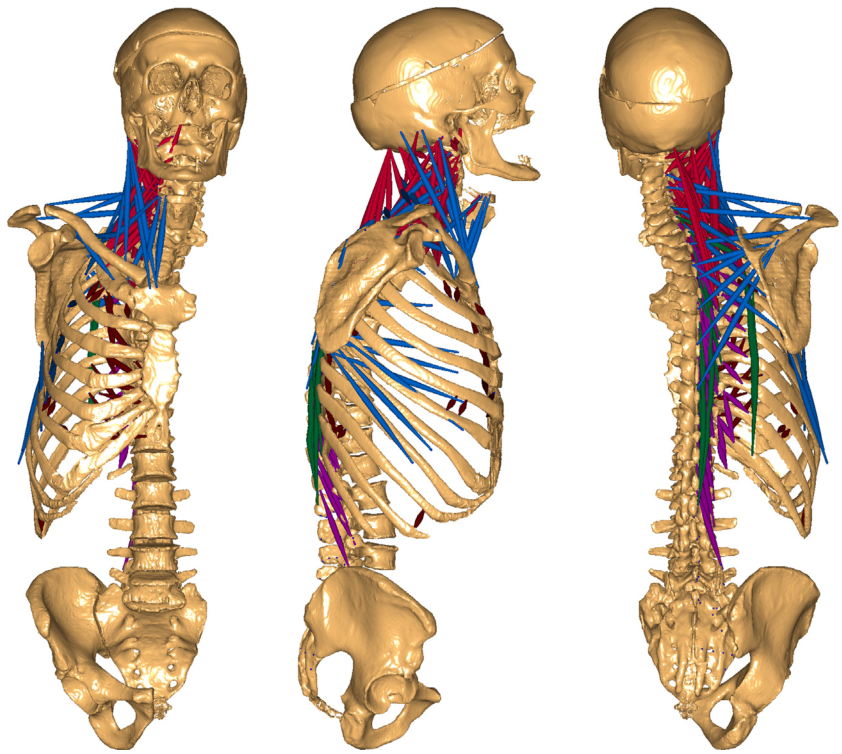

Fig. 3. From left to right: anterior, lateral, and posterior views of the measured musculo-skeletal system. Dissected muscles were highlighted in color: muscles of the thoracic spine (green), cervical spine (pale red), thoracic cage (dark red); deep muscles of the spine and ribcage (purple), and muscles connect spine to scapula, clavicle, and sternum (blue). (For interpretation of the references to color in this figure legend, the reader is referred to the web version of this article.)

Table 2
Comparison of the morphological parameters for the neck muscles measured in the present study with other anatomical studies. Standard deviations are shown in parenthesis.

Muscle	PCSA (cm^2)			ℓ_o^f (cm)			ℓ^s (μm)		
	Present	Kamibayashi[a]	Borst[b]	Present	Kamibayashi[a]	Borst[b]	Present	Kamibayashi[a]	Borst[b]
Iliocostalis cervicis	0.39	–	0.43	4.6	–	8.6	3.39	–	2.84
Levator scapulae	1.99	2.18 (0.80)	2.44	11.5	11.3 (3.1)	11.9	3.04	2.50 (0.40)	2.82
Longissimus capitis	0.59	–	0.75	6.9	–	7.0	2.81	–	2.52
Longissimus cervicis	1.34	–	1.59	3.2	–	7.2	3.70	–	2.79
Longus capitis	0.89	0.92 (0.35)	0.89	3.3	3.8 (1.0)	9.0	2.58	2.70 (0.40)	2.56
Obliquus capitis inferior	1.45	1.29 (0.54)	1.71	3.5	3.8 (0.8)	4.5	2.69	2.50 (0.40)	2.53
Obliquus capitis superior	0.33	1.03 (0.46)	0.92	1.8	2.5 (0.5)	4.3	3.16	2.60 (0.10)	3.06
Omohyoid	0.30	–	0.44	9.3	–	13.6	2.45	–	2.65
Rectus capitis anterior	0.20	–	0.08	1.0	–	1.8	2.63	–	2.49
Rectus capitis lateralis	0.10	–	0.78	0.6	–	1.9	2.63	–	2.58
Rectus capitis posterior major	1.04	0.93 (0.33)	0.54	2.8	3.7 (0.7)	3.9	2.83	2.40 (0.30)	2.50
Rectus capitis posterior minor	0.30	0.50 (0.19)	0.90	1.3	1.9 (0.2)	2.8	2.99	2.50 (0.30)	2.53
Rhomboideus minor[c]	3.35	5.84 (2.77)	0.96	8.9	7.2 (2.0)	9.0	3.19	2.50 (0.40)	2.50
Scalenus anterior	0.87	1.45 (1.23)	0.82	2.9	4.2 (1.3)	4.6	2.37	3.20 (0.60)	3.64
Scalenus medius	2.22	2.00 (0.73)	1.84	5.5	5.0 (0.8)	6.0	2.65	2.70 (0.40)	3.14
Scalenus posterior	0.42	1.55 (0.90)	0.89	5.2	6.2 (2.1)	5.8	2.48	2.60 (0.40)	3.03
Semispinalis capitis	3.06	5.40 (1.30)	4.27	7.4	6.8 (1.7)	9.8	3.06	2.50 (0.50)	2.86
Semispinalis cervicis	2.06	–	3.68	3.9	–	5.0	3.91	–	2.53
Serratus posterior superior	1.63	–	1.97	2.8	–	5.0	3.59	–	2.72
Splenius capitis[c]	2.03	4.26 (1.04)	2.50	6.9	9.5 (2.3)	10.2	3.16	2.50 (0.40)	2.82
Splenius cervicis[c]	1.23	4.26 (1.04)	0.99	6.1	9.5 (2.3)	10.2	3.55	2.50 (0.40)	2.78
Sternocleidomastoid	3.78	3.72 (0.91)	2.90	10.0	10.8 (0.9)	11.8	2.94	3.00 (0.20)	3.16
Sternohyoid	0.33	–	0.34	8.2	–	10.8	2.71	–	2.80
Sternothyroid	0.09	–	0.51	7.1	–	7.9	2.10	–	2.41
Thyrohyoid	0.33	–	0.60	2.7	–	3.8	2.46	–	3.13
Trapezius (descending part)[d]	2.90	1.96 (0.62)	3.54	8.4	8.4 (2.1)	10.6	2.86	2.70 (0.30)	3.04
Trapezius (transverse part)[d]	6.94	10.77 (2.38)	4.95	7.3	9.2 (1.8)	6.9	2.86	2.70 (0.30)	2.77

[a] References: Kamibayashi and Richmond (1998), three female and seven male embalmed cadavers (ages: 66–92 years).
[b] Borst et al. (2011), one embalmed male (age: 86 years, height: 1.71 m, mass: 75 kg). Optimal fiber length and sarcomere length data–of the individual elements–were averaged, and PCSAs were summed for comparison.
[c] Kamibayashi and Richmond (1998) reported data for the major and minor parts of the rhomboideus muscle together, and the cervicis and capitis parts of the splenius muscle together.
[d] The division of the trapezius muscle may be different between the studies.

data reported in the literature. Furthermore, the mean sarcomere lengths of some muscles were higher than those reported in Kamibayashi and Richmond (1998) and Borst et al. (2011). The mean sarcomere lengths of up to 3.91 μm were measured for the *cervicis* and *capitis* muscles which originated from the thoracic sixth vertebra and above. Moreover, the mean optimal fiber lengths were systematically lower compared to Borst et al. (2011), but very similar to the data in Kamibayashi and Richmond (1998). Similarly, the comparison of the muscle fiber lengths indicated lower fiber lengths in this study compared to Borst et al. (2011). We attributed this disparity to the differences between the heights of the cadavers measured (154 cm in this study and 171 cm in Borst et al. (2011)). We calculated optimal fiber lengths by dividing measured mean fiber lengths by the mean sarcomere lengths of the muscles and multiplying with 2.7 μm (assumed optimal sarcomere length for skeletal muscles (Breteler et al., 1999)). Therefore, the higher sarcomere lengths (in general) and the lower fiber lengths measured in this study explain the discrepancy between the optimal fiber lengths.

Several limitations affect the data presented in this study. Firstly, the architecture of the neck muscles may be affected due to scoliosis around this region (Fidler and Jowett, 1976). Secondly, we dissected the muscles only from one side of the cadaver. One then needs to assume about the skeletal geometry and muscle architecture for the other side when building a model. It is a common practice to create a left-right symmetrical musculo-skeletal model, however, the validity of such assumptions may be questionable (Bayoglu et al., 2016). Thirdly, measured architectural parameters of the muscles may deviate from *in vivo*. A mean shrinkage of 2% in muscle fiber lengths was reported when the muscles were fixed in isolation (Cutts, 1988). This suggests higher sarcomere and fiber lengths when measured *in vivo* and thus likely to cause slight changes in estimated optimal fiber lengths and physiological cross-sectional areas. Fourthly, this dataset was obtained from an older-adult male. Earlier studies discussed that isometric muscle strength declines with aging (Brooks and Faulkner, 1994). Häkkinen and Häkkinen (1991) suggested that the decline in isometric strength with aging may be associated with the decrease in the cross-sectional area of the muscle. Thus, we advise taking into account age-related changes in muscle morphology by adjusting the parameters of the Hill-type musculo-tendon models when this dataset is used to study younger populations (Thelen, 2003). For example, the isometric strengths of the muscles can be increased when studying young individuals. Moreover, some studies reported on the gender-related differences in muscle morphology (Morrow and Hosler, 1981; Lewis et al., 1986; Frontera et al., 1991). They asserted that men, in general, have greater upper and lower body strength compared to women. Therefore, when modeling female subjects (of similar age as the cadaver in this study), the isometric strengths of the muscles reported in the present study should be adjusted accordingly. Fifthly, we simplified the otherwise complex functions of muscles by dividing them into several muscle-tendon elements. This approach was a choice of modeling as such and required some assumptions. The details and underlying assumptions of this approach were described elsewhere (van der Helm and Veenbaas, 1991). Sixthly, the subcostales muscle was partially damaged on the right side during the resection of the intercostales muscle. For this reason, we collected the data for this muscle from the left side of the cadaver. Similarly, rectus capitis muscles (anterior and lateralis) were also measured on the left side as they were damaged during the resection of the neighboring muscles. Seventhly, intercostales muscles were measured only at three levels, between ribs 1 and 2, 5 and 6, and 9 and 10. In addition, levatores costarum longi (elements 2, 10, and 12) were measured only at the upper and lower rib levels. It may be reasonable to assume that measured parameters do not vary a lot between different levels for these muscles. Thus, interpolating or averaging of the reported data regarding these muscles can be used when modeling other levels. Lastly, measuring the coordinates of the attachments was impossible for the subcostales and transversus thoracis muscles as they were located inside the ribcage. Therefore, we identified their attachments at the bones and later visually defined their lines-of-action based on the pictures of the corresponding regions and anatomical illustrations given in Kim et al. (2015) and Gray et al. (1973).

The resection of the muscles around the cervical region of the spine revealed a notable anatomical variability in terms of the muscle attachments with the bones. A good example for this is the scalenus muscle group. Standard anatomy books such as Gray et al. (1973) describe the origin attachments of the scalenus anterior at the cervical third (C3) to sixth vertebrae (C6) and scalenus posterior at the C4–C6. Our measurements yet indicated the attachments at the C5–C7 and at the C3 vertebrae for these muscles, respectively. Such issues of anatomical variability are mentioned in Gray's book, Gray et al. (1973). We found similar variations for certain lumbar muscles in this cadaver as discussed in our earlier study (Bayoglu et al., 2017). This leads to the conclusion that certain care should be taken if a subject specific model is developed from a generic model or dataset.

Ward et al. (2009) discussed that the lumbar multifidus muscle acts as a stabilizer of the lumbar spine by producing considerable forces due to its architectural design associated with a high cross-sectional area and a low fiber length to muscle length ratio. Bojadsen et al. (2000) and Cornwall et al. (2011) mentioned on the architectural differences of the multifidus muscle in the lumbar and thoracic regions of the spine. Bojadsen et al. (2000) noted a pronounced increase in the tendinous tissue of this muscle in the thoracic region compared to the lumbar region. Furthermore, they postulated that the thoracic multifidus muscle (located on the antagonistic side) is exposed to large strains during the axial rotation of the spine and this seems related to the increase in tendinous tissue, which is much more resistant to deformation than the muscle tissue, in the upper thoracic spine. The morphology of the other deeper back muscles such as rotatores, levatores costarum, and semispinalis muscles has been investigated before, but only qualitatively (Cornwall et al., 2011; Langenberg and Jüschke, 1970). In this study, we also measured the transversospinal muscle group including levatores costarum and spinalis thoracis muscles and report new data for them. One common feature of these muscles (rotatores, levatores costarum, spinalis thoracis, and most elements of the multifidus) was that they were mostly tendinous in architecture, and their tendons ran from origin to insertion (musculo-tendon length being equal to tendon length) and were mixed with the muscle fibers. These muscle fibers either spanned the total length of the tendon or partly spanned (both of which are indicated in Table 1). The second common feature was that they had relatively small PCSAs implying that the active muscle force contribution will be small in these muscles. Such muscles can be modeled in several ways in computer models, for example as ligaments. In that case, the stiffness of the ligament, *i.e.* tendon, needs to be known. The stiffness can be calculated from the cross-sectional area, Young's modulus, and length of the tendon (Meijer et al., 2010). For this purpose, we additionally provide the tendon cross-sectional areas for these muscle elements. Due to their architectural design, we think that these muscles stabilize the spine at different regions preventing our joints from injury during excessive movements. Next to stabilizing function, they may also be responsible for protection by preventing overstretch of the muscle fibers. Further research is planned on the best way of modeling the actions of these muscles in musculo-skeletal models of the spine.

In our previous study, we presented an anatomical dataset for modeling the lumbar region of the spine (Bayoglu et al., 2017).

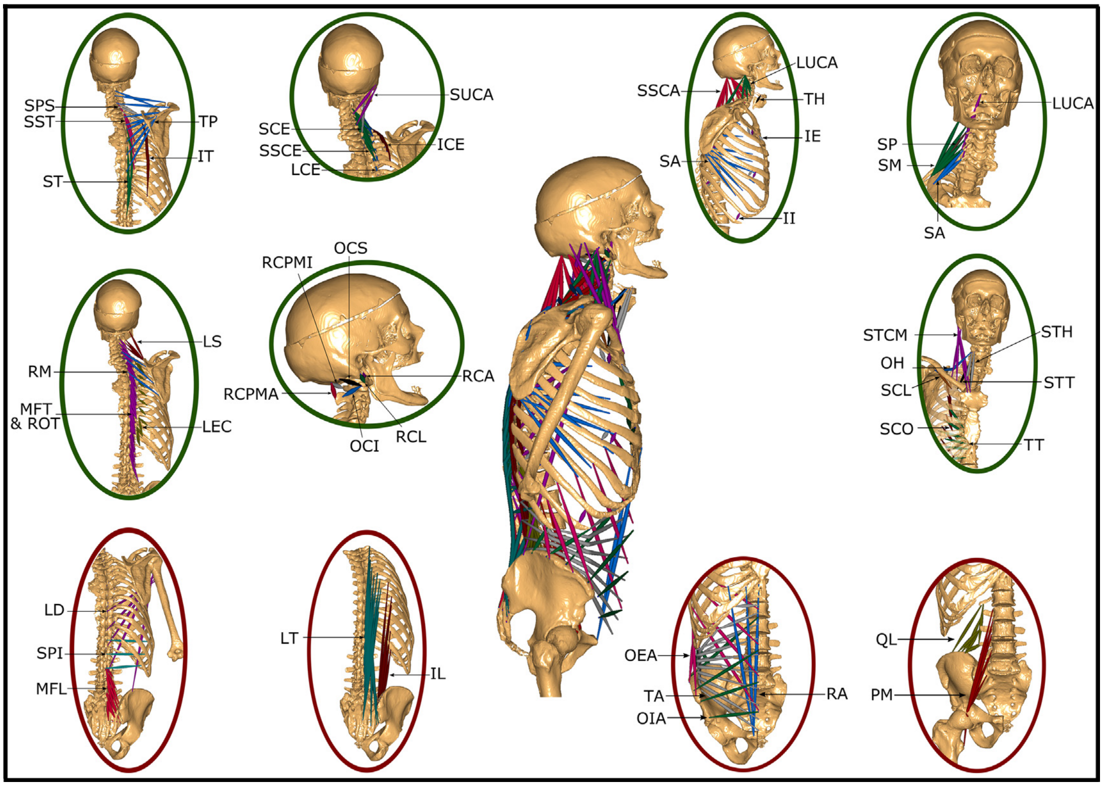

Fig. 4. The muscles measured in the complete anatomical dataset are highlighted. The muscles presented in this study are emphasized with green circles, whereas the muscles reported in our previous study with red circles (Bayoglu et al., 2017). See Appendix A.4 for the abbreviations used for the muscles. (For interpretation of the references to color in this figure legend, the reader is referred to the web version of this article.)

The dataset reported in this study was obtained from the same cadaver, therefore, it complements our earlier study and make a complete musculo-skeletal dataset for modeling the entire human spine. Because the complete dataset was obtained from a single cadaver, it is coherent and eliminates the uncertainties that come with combining musculo-skeletal data from different specimens (Horsman et al., 2007; Borst et al., 2011). All the bones and muscles obtained for the complete dataset are illustrated in Fig. 4. We hope that the complete dataset will further our understanding of the functioning of the healthy and pathological spine. All the data reported in this paper is shared with the scientific community through https://www.utwente.nl/en/et/bw/research/projects/twentespinemodel.

Conflict of interest

None of the authors have any financial or personal relationships with other people or organization that could inappropriately influence their work.

Acknowledgment

We acknowledge the financial supports by Fonds NutsOhra and the European Research Council 'the BioMechTools project'. Furthermore, we like to thank several colleagues for their help on this work, Vincenzo Carbone and Kenan Niu for useful discussions on musculo-skeletal modeling and motion capture systems, Alper Denasi for giving feedback on the manuscript, Frans Segerink for providing a laser and giving insights into laser diffraction technique, Andre Sprengers for his help during imaging sessions, and the Radiology Department and the Anatomy Department of the Radboud University Medical Center for their hospitality during the experiment. Finally, we thank Huub Maas from VU University of Amsterdam for sharing his expertise on sarcomere length measurements.

Appendix A. Supplementary material

Supplementary data associated with this article can be found, in the online version, at http://dx.doi.org/10.1016/j.jbiomech.2017.04.003.

References

Arjmand, N., Gagnon, D., Plamondon, A., Shirazi-Adl, A., Lariviere, C., 2009. Comparison of trunk muscle forces and spinal loads estimated by two biomechanical models. Clin. Biomech. 24 (7), 533–541.

Arnold, E., Ward, S., Lieber, R., Delp, S., 2010. A model of the lower limb for analysis of human movement. Ann. Biomed. Eng. 38 (2), 269–279.

Arshad, R., Zander, T., Dreischarf, M., Schmidt, H., 2016. Influence of lumbar spine rhythms and intra-abdominal pressure on spinal loads and trunk muscle forces during upper body inclination. Med. Eng. Phys. 38 (4), 333–338.

Bayoglu, R., Geeraedts, L., Groenen, K., Verdonschot, N., Koopman, B., Homminga, J., 2016. How valid are left-right symmetrical musculo-skeletal models? In: Proceedings of the 22nd Congress of the European Society of Biomechanics, 2016 July 10–13, Lyon, France.

Bayoglu, R., Geeraedts, L., Groenen, K.H., Verdonschot, N., Koopman, B., Homminga, J., 2017. Twente spine model: a complete and coherent dataset for musculo-skeletal modeling of the lumbar region of the human spine. J. Biomech. 53, 111–119.

Bogduk, N., Johnson, G., Spalding, D., 1998. The morphology and biomechanics of latissimus dorsi. Clin. Biomech. 13 (6), 377–385.

Bogduk, N., Macintosh, J.E., Pearcy, M.J., 1992a. A universal model of the lumbar back muscles in the upright position. Spine 17 (8), 897–913.

Bogduk, N., Pearcy, M., Hadfield, G., 1992b. Anatomy and biomechanics of psoas major. Clin. Biomech. 7 (2), 109–119.

Bojadsen, T., Silva, E., Rodrigues, A., Amadio, A., 2000. Comparative study of Mm. Multifidi in lumbar and thoracic spine. J. Electromyogr. Kinesiol. 10 (3), 143–149.

Borst, J., Forbes, P.A., Happee, R., Veeger, D.H., 2011. Muscle parameters for musculoskeletal modelling of the human neck. Clin. Biomech. 26 (4), 343–351.

Bresnahan, L., Fessler, R.G., Natarajan, R.N., 2010. Evaluation of change in muscle activity as a result of posterior lumbar spine surgery using a dynamic modeling system. Spine 35 (16), E761–E767.
Breteler, M., Spoor, C., Van der Helm, F., 1999. Measuring muscle and joint geometry parameters of a shoulder for modeling purposes. J. Biomech. 32 (11), 1191–1197.
Briggs, A.M., Van Dieën, J.H., Wrigley, T.V., Greig, A.M., et al., 2007. Thoracic kyphosis affects spinal loads and trunk muscle force. Phys. Ther. 87 (5), 595.
Brooks, S., Faulkner, J., 1994. Skeletal muscle weakness in old age: underlying mechanisms. Med. Sci. Sports Exerc. 26 (4), 432–439.
Bruno, A.G., Bouxsein, M.L., Anderson, D.E., 2015. Development and validation of a musculoskeletal model of the fully articulated thoracolumbar spine and rib cage. J. Biomech. Eng. 137 (8), 081003–081003-10.
Carbone, V., Fluit, R., Pellikaan, P., van der Krogt, M., Janssen, D., Damsgaard, M., Vigneron, L., Feilkas, T., Koopman, H., Verdonschot, N., 2015. TLEM 2.0 – a comprehensive musculoskeletal geometry dataset for subject-specific modeling of lower extremity. J. Biomech. 48 (5), 734–741.
Carbone, V., Van der Krogt, M., Koopman, H., Verdonschot, N., 2012. Sensitivity of subject-specific models to errors in musculo-skeletal geometry. J. Biomech. 45 (14), 2476–2480.
Carbone, V., van der Krogt, M., Koopman, H., Verdonschot, N., 2016. Sensitivity of subject-specific models to hill muscle-tendon model parameters in simulations of gait. J. Biomech. 49 (9), 1953–1960.
Cornwall, J., Stringer, M.D., Duxson, M., 2011. Functional morphology of the thoracolumbar transversospinal muscles. Spine 36 (16), E1053–E1061.
Cross, H., West, R., Dutson, T., 1981. Comparison of methods for measuring sarcomere length in beef semitendinosus muscle. Meat Sci. 5 (4), 261–266.
Cutts, A., 1988. Shrinkage of muscle fibres during the fixation of cadaveric tissue. J. Anat. 160, 75–78.
de Zee, M., Hansen, L., Wong, C., Rasmussen, J., Simonsen, E.B., 2007. A generic detailed rigid-body lumbar spine model. J. Biomech. 40 (6), 1219–1227.
Delp, S.L., Suryanarayanan, S., Murray, W.M., Uhlir, J., Triolo, R.J., 2001. Architecture of the rectus abdominis, quadratus lumborum, and erector spinae. J. Biomech. 34 (3), 371–375.
Erdemir, A., McLean, S., Herzog, W., van den Bogert, A.J., 2007. Model-based estimation of muscle forces exerted during movements. Clin. Biomech. 22 (2), 131–154.
Fidler, M., Jowett, R., 1976. Muscle imbalance in the aetiology of scoliosis. J. Bone Joint Surg. – Ser. B 58 (2), 200–201.
Frontera, W.R., Hughes, V.A., Lutz, K.J., Evans, W.J., 1991. A cross-sectional study of muscle strength and mass in 45- to 78-yr-old men and women. J. Appl. Physiol. 71 (2), 644–650.
Gray, H., Warwick, R., Williams, P.L., 1973. Gray's Anatomy. Longman.
Häkkinen, K., Häkkinen, A., 1991. Muscle cross-sectional area, force production and relaxation characteristics in women at different ages. Eur. J. Appl. Physiol. Occup. Physiol. 62 (6), 410–414.
Han, K.-S., Rohlmann, A., Zander, T., Taylor, W., 2013. Lumbar spinal loads vary with body height and weight. Med. Eng. Phys. 35 (7), 969–977.
Horsman, M.K., Koopman, H., Van der Helm, F., Prosé, L.P., Veeger, H., 2007. Morphological muscle and joint parameters for musculoskeletal modelling of the lower extremity. Clin. Biomech. 22 (2), 239–247.
Ignasiak, D., Dendorfer, S., Ferguson, S., 2016. Thoracolumbar spine model with articulated ribcage for the prediction of dynamic spinal loading. J. Biomech. 49 (6), 959–966.
Kamibayashi, L., Richmond, F., 1998. Morphometry of human neck muscles. Spine 23 (12), 1314–1323.
Kim, J.-H., Won, H.-S., Chung, I.-H., Kim, I.-B., 2015. The enigmatic subcostal muscle: anatomical study with application to spine and chest pain syndromes and avoidance of confusion on imaging. Clin. Anat. 28 (8), 1017–1021.
Langenberg, W., Jüschke, S., 1970. Morphology and innervation of the Mm. levatores costarum and their relation to the Mm. intertransversarii. Z. Anat. Entwicklungs. 130 (3), 255–264.
Lewis, D., Kamon, E., Hodgson, J., 1986. Physiological differences between genders implications for sports conditioning. Sports Med. 3 (5), 357–369.
Macintosh, J.E., Bogduk, N., 1991. The attachments of the lumbar erector spinae. Spine 16 (7), 783–792.
Macintosh, J.E., Valencia, F., Bogduk, N., Munro, R.R., 1986. The morphology of the human lumbar multifidus. Clin. Biomech. 1 (4), 196–204.
Meijer, G.J., Homminga, J., Hekman, E., Veldhuizen, A., Verkerke, G., 2010. The effect of three-dimensional geometrical changes during adolescent growth on the biomechanics of a spinal motion segment. J. Biomech. 43 (8), 1590–1597.
Modenese, L., Ceseracciu, E., Reggiani, M., Lloyd, D., 2016. Estimation of musculotendon parameters for scaled and subject specific musculoskeletal models using an optimization technique. J. Biomech. 49 (2), 141–148.
Morrow Jr., J.R., Hosler, W., 1981. Strength comparisons in untrained men and trained women athletes. Med. Sci. Sports Exerc. 13 (3), 194–197.
Phillips, S., Mercer, S., Bogduk, N., 2008. Anatomy and biomechanics of quadratus lumborum. Proc. Inst. Mech. Eng. Part H: J. Eng. Med. 222 (2), 151–159.
Putzer, M., Ehrlich, I., Rasmussen, J., Gebbeken, N., Dendorfer, S., 2016. Sensitivity of lumbar spine loading to anatomical parameters. J. Biomech. 49 (6), 953–958.
Thelen, D.G., 2003. Adjustment of muscle mechanics model parameters to simulate dynamic contractions in older adults. J. Biomech. Eng. 125 (1), 70–77.
Valente, G., Pitto, L., Testi, D., Seth, A., Delp, S., Stagni, R., Viceconti, M., Taddei, F., 2014. Are subject-specific musculoskeletal models robust to the uncertainties in parameter identification? PLoS ONE 9 (11).
van der Helm, F., Veenbaas, R., 1991. Modelling the mechanical effect of muscles with large attachment sites: application to the shoulder mechanism. J. Biomech. 24 (12), 1151–1163.
Vasavada, A.N., Li, S., Delp, S.L., 1998. Influence of muscle morphometry and moment arms on the moment-generating capacity of human neck muscles. SPINE 23 (4), 412–422.
Ward, S., Kim, C., Eng, C., Gottschalk IV, L., Tomiya, A., Garfin, S., Lieber, R., 2009. Architectural analysis and intraoperative measurements demonstrate the unique design of the multifidus muscle for lumbar spine stability. J. Bone Joint Surg. – Ser. A 91 (1), 176–185.
Zajac, F., 1989. Muscle and tendon: properties, models, scaling, and application to biomechanics and motor control. Crit. Rev. Biomed. Eng. 17 (4), 359–411.